IOPscience iopscience.iop.org

Home Search Collections Journals About Contact us My IOPscience

First-principles electronic structure calculations for incommensurately modulated calaverite

This article has been downloaded from IOPscience. Please scroll down to see the full text article.

1990 J. Phys.: Condens. Matter 2 4829

(http://iopscience.iop.org/0953-8984/2/22/005)

View the table of contents for this issue, or go to the journal homepage for more

Download details:
IP Address: 171.66.16.96
The article was downloaded on 10/05/2010 at 22:14

Please note that terms and conditions apply.

J. Phys.: Condens. Matter **2** (1990) 4829–4847. Printed in the UK

First-principles electronic structure calculations for incommensurately modulated calaverite

B C H Krutzen and J E Inglesfield
Institute for Theoretical Physics, Faculty of Science, University of Nijmegen, Toernooiveld, 6525 ED Nijmegen, The Netherlands

Received 18 January 1990

Abstract. Fully relativistic first-principles electronic structure calculations of both the average structure and a supercell approximation of silver-free incommensurately modulated calaverite ($AuTe_2$) are presented. The differences between the results of both calculations are relatively small for the occupation numbers and the density of states, but quite dramatic for the shape of the Fermi surface. From the occupation numbers it is concluded that a previously proposed idea for explaining the modulation, based on mixed valencies for the gold atoms, is probably not applicable. The calculated Fermi surface of the average structure shows that the modulation cannot be understood in terms of Fermi-surface nesting either. The density of states in the supercell approximation compares very favourably with recently obtained x-ray photoelectron spectroscopy data. A rigid-potential calculation shows that the integral of the one-electron valence energies for the supercell is substantially more negative than the corresponding energy for the average structure, while the electrostatic energy difference has the opposite sign but is much smaller. This provides a qualitative indication of the electronic instability of the average structure with respect to the modulation of the supercell. Finally we conclude that Te s-like states a (Te p–Au d)-like complex dominate the energetics of the modulation.

1. Introduction

Recently there has been a revival of interest in the incommensurate gold-containing mineral calaverite $Au_{1-x}Ag_xTe_2$ ($0 \leqslant x \leqslant 0.15$) [1–7], which was of morphological interest already at the beginning of this century [8–11]. The revival is caused by the discovery that this mineral belongs to the class of incommensurately modulated structures [1]. The present paper deals with its electronic structure, which is of interest from two points of view. First, there is hope that detailed knowledge of the electronic structure will provide insight into the driving forces of the modulation. Secondly, the electronic structure is fundamental for calculations of physical properties of various kinds and thus for the study of the influence of the incommensurability on these properties.

The calculation of the electronic structure for incommensurately modulated crystals is inhibited by the difficulty of handling an infinitely large unit cell, as is the case with quasi-crystals. The usual way to deal with this problem is to study a specific series of periodic approximations to the crystal structure and to deduce conclusions for the limiting case of the incommensurate structure from the trends in the approximate results. This technique has provided considerable understanding of spectra and wavefunctions,

0953-8984/90/224829 + 19 $03.50 © 1990 IOP Publishing Ltd

mostly of one-dimensional model systems [4]. One-dimensional systems are more easy to study because of the availability of simple calculation techniques, such as the transfer matrix method. The most striking features for one-dimensional incommensurate systems are point-like parts in the spectrum and the (associated) occurrence of localised states. It should be noted, however, that the localised states are nothing other than electrons trapped by the potential, which is obviously much more difficult in higher dimensions. In this paper we will apply the study of periodic approximations to calaverite.

The character of the electron orbits that enter the chemical bonding in calaverite, especially the Au 5d electrons, forces us to use relativistic self-consistent band-structure techniques. As a consequence of the time-consuming nature of these techniques, only the average structure and the first rational approximant (or periodic approximation), involving a supercell, which is four times as big as the unit cell of the average structure, are practically accessible.

The calculations have been performed with the use of the *ab initio* relativistic augmented spherical-wave (RASW) method [12]. A short description of this method will be given in section 2. In section 3 the relevant crystal structures are discussed. The results of the calculations for the average structure can be found in section 4, and those for the supercell structure in section 5. In section 6 the calculated density of states for the supercell calculation is compared with the results of experimental x-ray photoelectron spectroscopy (XPS). Several possible driving forces of the modulation are discussed in section 7 and the conclusions of the paper are presented in section 8.

2. The method of calculation

In view of the necessity for the self-consistent treatment of all relativistic terms in the electron Hamiltonian and the requirement for efficiency because of the large number of atoms in the unit cell, the choice was made for an *ab initio* local density calculation making use of the atomic sphere approximation (ASA) to the crystal potential. A suitable procedure of this kind is provided by the RASW scheme introduced by Takeda in 1979 [12]. This scheme is a fully relativistic version of the well known ASW method of Williams *et al* [13] and can be considered equivalent to similar generalisations of the linear muffin-tin orbitals (LMTO) method [14]. Recently we generalised the RASW method to include spin polarisation [15] and this newly developed code was used to perform the calculations presented in this paper, although the calculations are not spin polarised. Since both the original Takeda paper [12] and our paper presented the generalisation [15] contain a fairly detailed description of the RASW method, we will restrict ourselves in this paper to a general discussion of the approximations involved.

The many-electron problem is reduced in a standard way to single-particle equations using density-functional theory. The local density approximation is applied using the exchange and correlation function of Perdew and Zunger [16], who fitted their function to Monte Carlo results of Ceperley and Alder [17]. The self-consistent field crystal potential is treated in the atomic sphere approximation, in which space is divided into atomic spheres and the remaining interstitial region. Inside the atomic spheres the potential is spherically averaged and in the interstitial region the potential is taken constant. The interstitial space is eliminated almost entirely by choosing the sphere radii (Wigner–Seitz radii) such that the sum of the sphere volumes in the unit cell is equal to the volume of the unit cell. This procedure will cause an unacceptably large overlap of atomic spheres if the crystal structure under consideration is not almost close-packed.

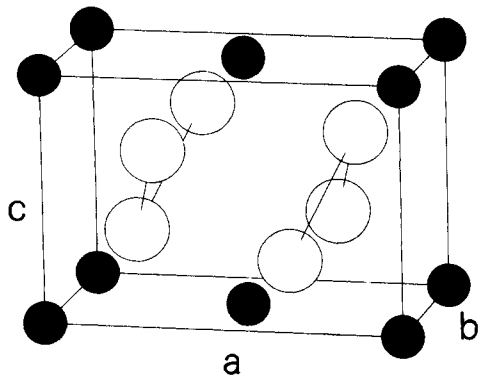

Figure 1. The unit cell of the average structure containing six atoms listed in table 2. Small full circles represent Au, large open circles Te atoms. The empty spheres added in the calculation have been left out for clarity. The zig-zag chains of Te atoms are indicated by the lines joining the Te atoms. The directions of the primitive vectors $\boldsymbol{a}$, $\boldsymbol{b}$, $\boldsymbol{c}$ are also shown.

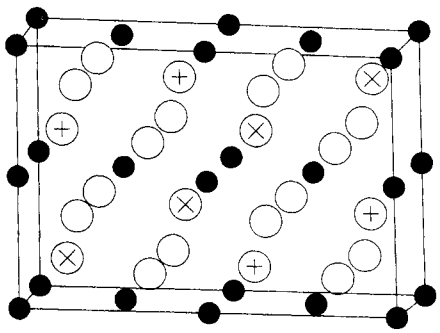

Figure 2. The unit cell for the superstructure, according to the positions in table 4. The cell contains four unit cells of the average structure (see figure 1). Inside the Te atoms the phase of the modulation (if non-zero) is shown: + and × indicate $+\frac{1}{4}$ and $-\frac{1}{4}$ respectively. The Au atoms in the centred positions have a nearly linear coordination, as in the average structure, because four neighbours stay in place and two others move perpendicular to the bond lines. The Au atoms on the corners of the cell and their equivalent atoms have now, due to the modulation, a nearly square coordination, because two neighbouring Te atoms are shifted towards them, two away from them, while two others stay in place. Empty spheres have been left out for clarity.

In such cases this problem is circumvented by the insertion of empty atomic spheres. These empty spheres do not contain nuclear charge nor core electrons but some valence charge will flow into them in the self-consistency process. In this way a large part of the space is treated properly and the overlap of the spheres, which is neglected in the calculation, remains acceptable. The remaining interstitial charge is accounted for in the overlap and Hamiltonian matrices in a standard way. The integral over the unit cell of this contribution is converted into a sum of integrals over the atomic sphere boundaries using Green's theorem for the basis functions and their energy derivatives [13]. Since the determination of the crystal potential does not allow for interstitial charge, it has to be renormalised into the spheres at every iteration of the self-consistency procedure. As the potential approximation is particularly crude in the interstitial region, the amount of interstitial charge appearing in the calculation is one measure of the applicability of the atomic sphere approximation.

The electrons in the crystal are divided into core and valence electrons, which are treated in different ways. The core electrons, which do not overlap substantially, are treated in an atomic type of approach. The valence electrons are represented by functions that form the basis of the overlap and Hamiltonian matrices. These functions are Bloch sums over the atom-centered RASW functions. In the formulation of our previous paper [15], these atom-centred functions consist in the interstitial region of four-component spinors with an outgoing spherical Hankel function multiplied by a *pure spin* Pauli spinor for their *large* components. The small components, which are of a complicated form,

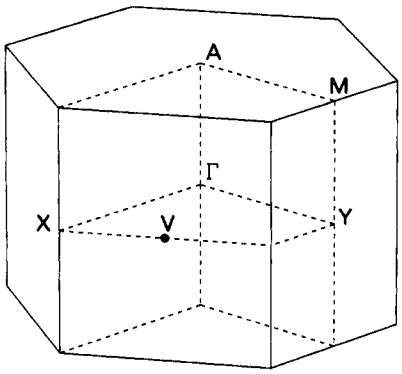

Figure 3. The Brillouin zone of the average structure (C2/m). The irreducible wedge is contained between the broken lines.

are determined by the requirement that the four-spinor is a solution to the Dirac equation with a constant potential. These interstitial functions are matched onto (augmented with) solutions of the radial Dirac equations inside all the atomic spheres. The entire atom-centred function is in this way specified by the orbital moment of the Hankel function and the orbital moment of the radial Dirac equations, which are taken equal, and by the principal quantum number of the radial Dirac equation, which determines the number of nodes of the function. Although the principal quantum number and orbital momentum are thus used to specify the atom-centred valence functions, it should be noted that the actual form of these functions, which changes during the self-consistency process, is quite different from that of the corresponding atomic orbitals. For Au we include the 6s, 6p and 5d functions and for Te the 5s, 5p and 5d functions in the basis for the band matrix.

In order to find the matching conditions for the augmentation of the basis functions, a spherical Hankel function centred on one atom is expanded in terms of spherical Bessel functions on all the other atoms, using the expansion theorem of the original ASW method [13]. Each expansion involves in principle an infinite number of orbital momenta for the Bessel functions. It can be shown, however, that the expansion coefficients decrease with increasing orbital momentum. Therefore the expansion is truncated after a finite orbital momentum value l, which we choose for both Au and Te functions to be $l = 3$. The valence functions associated with the inserted empty spheres are taken to be 1s and 2p and the expansion of these functions is truncated at $l = 2$.

Finally, the Brillouin zone integral has to be performed at each iteration. For the self-consistency process we use a simple zero-order sampling technique in the irreducible part with symmetry-determined weights. The density of states (DOS) was calculated with the more accurate first-order tetrahedron method. In this method the irreducible part of the Brillouin zone is divided into a number of irregular tetrahedra (simplices), which again are divided into small tetrahedra by repeated application of a fixed division procedure. The resulting tetrahedra cover the irreducible part completely and have approximately equal volumes. The band problem is solved for the set of corners shared by these tetrahedra. The contribution to the DOS for each tetrahedron is then calculated analytically using a linear expression for the band energies, which is obtained by interpolation between the band energies at the four corners of the tetrahedron under consideration.

3. The incommensurate crystal structure and its approximants

The class of incommensurately modulated structures is closely related to the class of quasi-crystals and both types can be described by a single formalism involving higher-dimensional periodicity. In both types of structure the long-range order is in principle perfect, in spite of the absence of lattice periodicity, giving rise to new types of diffraction patterns with sharp spots. In mathematical terms these structures are characterised by the property that the Fourier transform of the charge density (and the crystal potential) consists of components belonging to a set of integral linear combinations of more than three reciprocal lattice vectors. For crystals such as calaverite with a periodic average structure and an incommensurate modulation with only one wavevector, the reciprocal structure is spanned by four basis vectors [4]. In three dimensions these basis vectors are necessarily dependent with respect to the real numbers, but they are independent with respect to the rational numbers (*rationally* independent). It is possible to use the basis vectors to embed the three-dimensional non-periodic structure in a four-dimensional *periodic* structure [4]. The three-dimensional aperiodicity of the system is caused by the irrational relation of one or more components of the basis vectors. It is possible to recover the three-dimensional periodicity if one or more of the basis vectors are slightly changed such that the vectors become rationally dependent, and in that way we obtain a so-called rational approximant. For these periodic approximations the conventional electronic structure calculation techniques—using Bloch's theorem—can be applied. This procedure will be chosen in the rest of this paper. In order to find appropriate approximants, it is useful to consider briefly the general situation for incommensurate crystals.

A distinction between incommensurately modulated structures and quasi-crystals can be seen from their x-ray diffraction patterns. For the former there always exists a sub-pattern of high-intensity spots, the main reflections, corresponding to a real space periodic structure, which is called the average structure. In addition, there is a set of peaks, the satellite spots, grouped around the high-intensity spots, with distances to the main reflections that are not commensurate with the periodicity of the average structure. The satellite reflections can be shown to occur because of displacive or other incommensurate modulations of the average structure. Often the amplitude of the modulation is not too big and the structure can be adequately described by a perturbation of the average structure. For the quasi-crystalline structures, however, such a division of the diffraction pattern, and thus of the structure, into an average structure and one or more incommensurate modulations, is in general not possible. In the following a description of the average structure and the modulations for calaverite are presented as well as the rational approximant used in the calculation.

The average structure of calaverite was determined by Tunell and Pauling [18]. Its space group is C2/m (*International Tables*, number 12). The vertices and corresponding centred positions of the almost rhombohedrally shaped unit cell (monoclinic angle 90.04°) are occupied by gold atoms, while the space between the gold planes is filled with two tilted ziz-zag chains of tellurium atoms in the direction of the monoclinic twofold crystallographic axis. Figure 1 shows the unit cell and the direction of the conventional unit vectors $\boldsymbol{a}$, $\boldsymbol{b}$ and $\boldsymbol{c}$. The primitive lattice translations and the atomic positions in the unit cell are listed in tables 1 and 2, together with the Wigner–Seitz radii of the atomic spheres used in the calculation, including the empty spheres mentioned in the previous section, which are inserted to obtain a reasonable space filling.

Accurate determinations of the incommensurate modulation were performed by Schutte and de Boer [5]. There is a displacive as well as an occupation modulation

Table 1. Primitive lattice translations (row vectors) of the average structure in atomic units.

	Primitive lattice vectors		
1	6.7977	−4.1710	0.0000
2	6.7977	4.1710	0.0000
3	0.0000	0.0000	9.5810

Table 2. Atomic positions in the unit cell (row vectors) of the average structure and their Wigner–Seitz (ws) radii in atomic units. Inserted empty spheres are indicated by e.s.

	Atom	Sym. class	Position (x, y, z)			ws radius
1	Au	1	0.000	0.000	0.000	2.9651
2	Te	2	9.371	0.000	2.762	2.9651
3	Te	2	4.224	0.000	6.819	2.9651
4	e.s.	3	0.000	0.000	4.791	2.5796
5	e.s.	4	4.503	0.000	2.019	2.5796
6	e.s.	4	9.093	0.000	7.562	2.5796

Table 3. Primitive lattice translations (row vectors) of the superstructure in atomic units

	Primitive latice vectors		
1	13.5954	0.0000	9.5810
2	13.5954	0.0000	−9.5810
3	0.0000	8.3420	0.0000

with the same incommensurate wavevector $\boldsymbol{q} = -0.4076\boldsymbol{a}^* + 0.4479\boldsymbol{c}^*$, where asterisks denote reciprocal vectors. The occupation modulation leads to partial occupation of the gold positions, with a probability of finding Ag atoms on Au sites of at most 0.15. The displacive modulation is most important on tellurium sites with an amplitude of approximately 0.76 au parallel to the twofold axis and primarily a first-order harmonic character. There is also a small modulation of the gold and silver positions ($\simeq$0.08 au).

Given the time-consuming nature of the chosen method of calculation, we could not treat more than the displacive modulation of the tellurium atoms. The lowest-order rational approximant distinct from the zero-order average structure, has $\boldsymbol{q} = -\frac{1}{2}\boldsymbol{a}^* + \frac{1}{2}\boldsymbol{c}^*$, such that the unit cell becomes four times as large as that of the average structure. The relative phases of the Te atoms can be approximated by multiples of 1/4 in the same way as we treated $\boldsymbol{q}$, while the actual phase values for the approximated $\boldsymbol{q}$ are ± 0.20, ± 0.05 and so on. The phase offset, which should be fixed for a commensurate approximation, is chosen such that the modulation effect is maximal. The supercell now contains the two limiting environments of Au atoms found in the actual incommensurate structure, namely the nearly linear and the nearly square planar coordination by Te atoms. In figure 2 the ac plane of the supercell is shown, with the displaced tellurium atoms and the two different Au coordinations. The primitive lattice translations and the positions of the atoms and empty spheres are listed in tables 3 and 4. The positions of the empty

Table 4. Atomic positions in the unit cell (row vectors) of the superstructure and their Wigner–Seitz (WS) radii in atomic units. Inserted empty spheres are indicated by e.s.

	Atom	Sym. class	Position (x, y, z)			WS radius
1	Au	1	0.000	0.000	0.000	2.9651
2	Au	1	0.000	0.000	−9.581	2.9651
3	Au	2	6.798	4.171	−9.581	2.9651
4	Au	2	6.798	4.171	0.000	2.9651
5	Te	3	4.224	0.000	6.819	2.9651
6	Te	3	4.224	0.000	−2.762	2.9651
7	Te	3	9.371	0.000	−6.819	2.9651
8	Te	3	9.371	0.000	2.762	2.9651
9	Te	4	2.574	4.841	2.762	2.9651
10	Te	4	2.574	3.501	−6.819	2.9651
11	Te	4	11.022	3.501	−2.762	2.9651
12	Te	4	11.022	4.841	6.819	2.9651
13	e.s.	5	0.000	0.000	4.791	2.5796
14	e.s.	5	0.000	0.000	−4.791	2.5796
15	e.s.	6	6.798	4.171	4.791	2.5796
16	e.s.	6	6.798	4.171	−4.791	2.5796
17	e.s.	7	4.503	0.000	−7.562	2.5796
18	e.s.	7	4.503	0.000	2.019	2.5796
19	e.s.	7	9.093	0.000	7.562	2.5796
20	e.s.	7	9.093	0.000	−2.019	2.5796
21	e.s.	8	11.301	4.171	−7.562	2.5796
22	e.s.	8	11.301	4.171	2.019	2.5796
23	e.s.	8	2.295	4.171	7.562	2.5796
24	e.s.	8	2.295	4.171	−2.019	2.5796

spheres are not modulated because of symmetry considerations. The space group for this superstructure is P2/c and the reciprocal lattice has space group P2/m (*International Tables*, number 13 and 10, respectively).

4. Results for the average structure

Self-consistent results with a cubic mesh of 100 $\boldsymbol{k}$-vectors in the irreducible wedge of the Brillouin zone (figure 3) have been obtained to an accuracy of 10^{-4} electrons per atom. The density of states was calculated with 2048 tetrahedra in the irreducible wedge. The interstitial charge was 0.42 electrons per unit cell, i.e. 1.8% of the 23 valence electrons, which indicates a reasonable space filling. The partial occupation numbers can be found in table 5, the bands along symmetry directions in the Brillouin zone in figure 4, and the total and partial density of states (DOS) in figure 5.

The overall picture of the band structure is quite simple: From −13.4 to −10.0 eV with respect to the Fermi level the Te 5s bands are well separated from the rest of the valence bands. The Au 5d contributions extend from −6.5 to −4.0 eV with a small, extended tail up to +1.5 eV. The main contribution to the DOS at the Fermi energy comes from the Te 5p states with small contributions from Au 5d and empty sphere states. Although the pure spin character of the states is removed by the implicit spin–

Table 5. Atomic charges in the unit cell of the average structure. Note the positive sign of the electron charge. The valence charge is split into eigenstates, labelled with κ, of the operator $1 + \sigma L$. With $\kappa = -l - 1$ for $j = l + \frac{1}{2}$ and $\kappa = l$ for $j = l - \frac{1}{2}$ the listed contributions can be added to obtain the usual s, p, d and f parts.

Sym. class	1	2	3	4
Atom	Au	Te	e.s.	e.s.
Number of atoms	1	2	1	2
Nuclear charge	−79	−52	0	0
Core charge	68.00	46.00	0.00	0.00
Valence charge				
$\kappa = -1$	0.87	1.72	0.33	0.37
$\kappa = -2$	0.41	1.75	0.24	0.29
$\kappa = +1$	0.29	1.07	0.13	0.15
$\kappa = -3$	5.36	0.10	0.09	0.11
$\kappa = +2$	3.70	0.07	0.06	0.07
$\kappa = -4$	0.03	0.02		
$\kappa = +3$	0.02	0.02		
Total electrons	78.69	50.75	0.85	0.98
Total atom	−0.31	−1.25	+0.85	+0.98

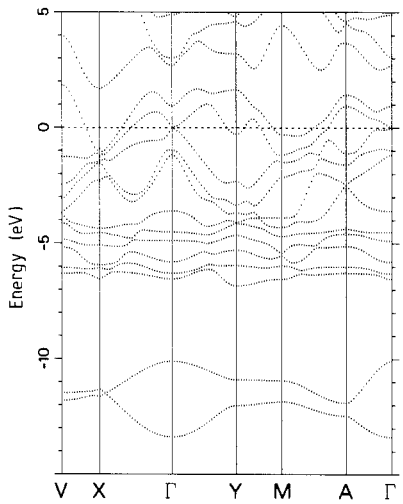

Figure 4. Energy bands of the average structure along the symmetry directions indicated in figure 3. The horizontal broken line is the Fermi level.

orbit coupling in the Dirac equation, the energy bands are still twofold degenerate due to the inversion symmetry of the average structure (Kramers degeneracy). The bands 23/24 and 25/26 cross the Fermi level, while the bands 21/22 approach the Fermi level at Γ. Between bands 25/26 and 27/28 there is a gap of nearly 2 eV over a large portion of the Brillouin zone, creating a minimum in the total DOS at +1.8 eV.

5. Results for the superstructure

The self-consistent calculation has been carried out with a cubic mesh of 30 $\boldsymbol{k}$-vectors in the irreducible wedge of the Brillouin zone. This gives approximately the same density

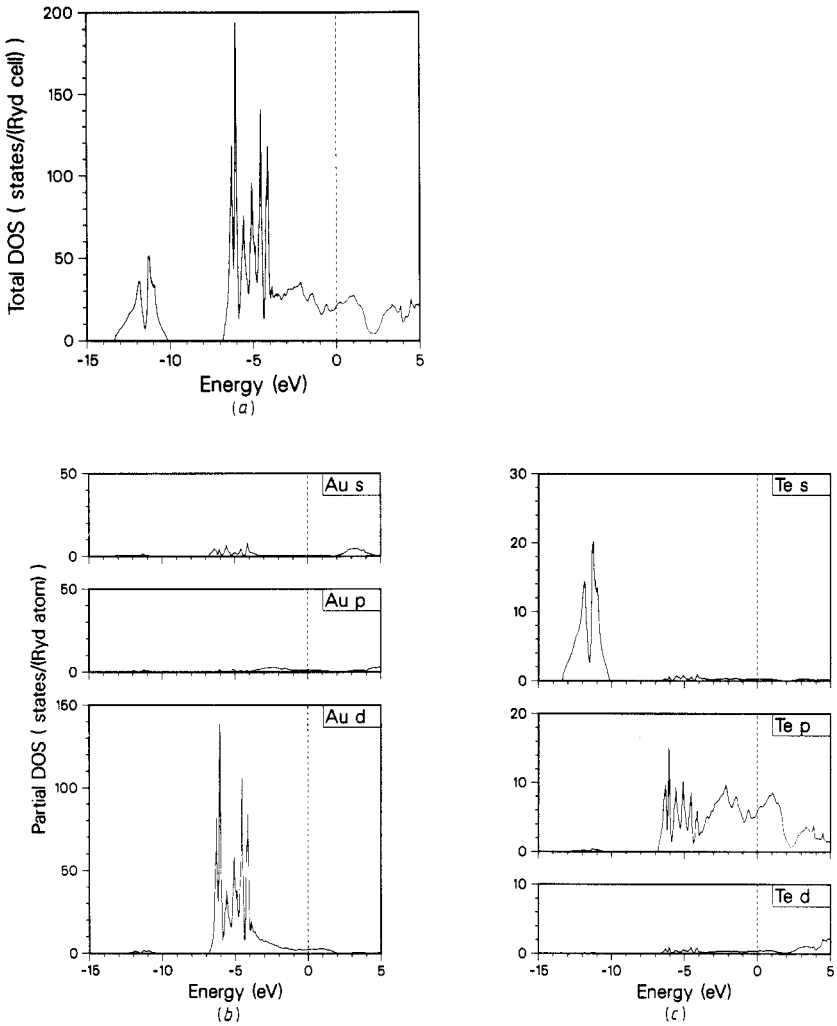

Figure 5. The density of states (DOS) for the average structure. In (*a*) the total DOS is shown and in (*b*) and (*c*) the partial DOS for the Au- and Te-centred crystal states.

of ***k***-vectors as used in the sampling of the wedge for the average structure, because the wedge of the superstructure is four times smaller than that of the average structure. The DOS calculation has been performed with 1024 tetrahedra in the irreducible wedge. The same convergence criteria as in case of the average structure have been used. The interstitial charge for this calculation is 2.5 electrons per unit cell, i.e. 2.7% of the 92 valence electrons. This is somewhat more than for the average structure, but still quite acceptable.

The occupation numbers for the symmetry-inequivalent atoms are listed in table 6. The differences with the corresponding atoms in the average structure are small. The energy bands (figure 7) plotted along the symmetry directions of the irreducible wedge as indicated in figure 6 show greater differences compared with the average structure, at least in the neighbourhood of the Fermi level. The bands are still doubly degenerate

Table 6. Atomic charges in the unit cell of the superstructure. Note the positive sign of the electron charge.

Sym. class	1	2	3	4	5	6	7	8
Atom	Au	Au	Te	Te	e.s.	e.s.	e.s.	e.s.
Number of atoms	2	2	4	4	2	2	4	4
Nuclear charge	−79	−79	−52	−52	0	0	0	0
Core charge	68.00	68.00	46.00	46.00	0.00	0.00	0.00	0.00
Valence charge								
$\kappa = -1$	0.87	0.87	1.71	1.70	0.35	0.32	0.40	0.36
$\kappa = -2$	0.45	0.40	1.74	1.72	0.26	0.24	0.32	0.28
$\kappa = +1$	0.32	0.28	1.06	1.05	0.14	0.12	0.16	0.15
$\kappa = -3$	5.34	5.35	0.10	0.10	0.10	0.09	0.13	0.10
$\kappa = +2$	3.67	3.68	0.07	0.07	0.06	0.06	0.08	0.06
$\kappa = -4$	0.04	0.03	0.02	0.03				
$\kappa = +3$	0.03	0.02	0.02	0.02				
Total electrons	78.71	78.63	50.72	50.70	0.90	0.83	1.09	0.96
Total atom	−0.29	−0.37	−1.28	−1.30	+0.90	+0.83	+1.09	+0.96

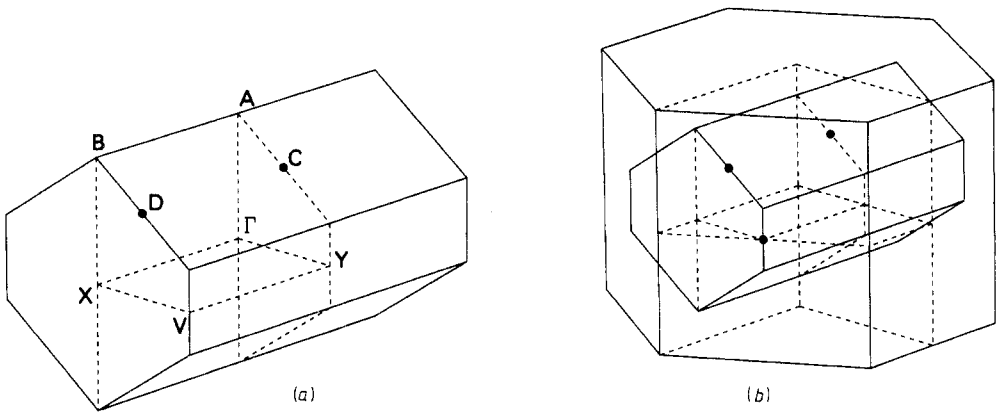

Figure 6. The Brillouin zone of the superstructure (P2). The symmetry lines and irreducible part are shown in (*a*), the relative position with respect to the Brillouin zone of the average structure (figure 3) is plotted in (*b*).

because of the inversion symmetry of the supercell, but the splitting of bands due to the modulation can clearly be seen. The effect of the change in the energy bands on the Fermi surface is in fact quite dramatic. Therefore, the interpretation of experimental data, such as de Haas–van Alphen oscillations, can clearly not be based on the Fermi surface of the average structure, and this sensitivity to the modulation implies that we should also be very cautious about using the Fermi surface of the supercell.

The total and partial DOS of the supercell are shown in figure 8. The splitting of the bands in the supercell is largely integrated out and the remaining splittings are certainly too small to observe experimentally, except for the new peak structure that appeared at +4.5 eV. It would be interesting to see whether this can be observed in an x-ray absorption spectroscopy experiment. The new peak is largely due to states situated on empty spheres and Te atoms.

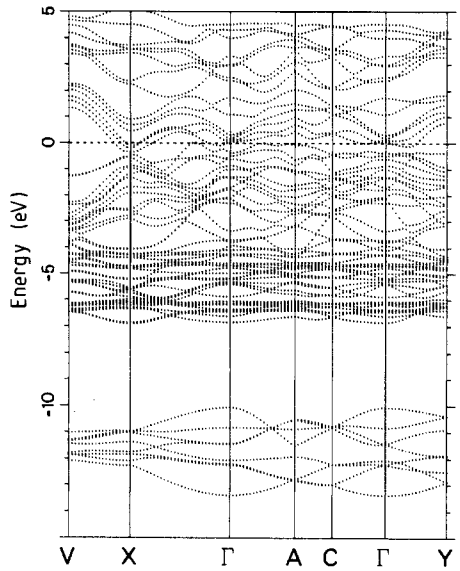

Figure 7. Energy bands of the superstructure along the symmetry directions indicated in figure 6(*a*). The horizontal broken line is the Fermi level.

6. The XPS valence spectrum

The calculated valence DOS for the supercell structure can be compared with the valence spectra from x-ray photoelectron spectroscopy (XPS) measurements performed by van Triest [19] with an Al Kα source of 1486.6 eV. We broaden the calculated DOS of figure 8(*a*) to include lifetime effects and finite experimental resolution with a Lorentzian convolution with a full width at half-maximum (FWHM) of $0.50 + 0.1(E_F - E)$ eV and Gaussian convolution with a constant FWHM of 0.50 eV. In figure 9(*a*) this broadened DOS is compared with experiment. The experimental and calculated Fermi level are lined up and the experimental curve is scaled down to match the calculated maximum near -5 eV.

The double peak structure due to the Au d-like states at -6 eV is in excellent agreement with experiment. Also the gap, reduced by broadening, near -9 eV and the Te s-like states at -12 eV are found at the same energies as in the experiment. The remaining discrepancies can be found in the peak heights and the relative contribution of the Te p-like states. They can be attributed to the different scattering cross sections of the different crystal functions contributing to the total experimental spectrum, which are neglected in the calculation, but should in fact be incorporated through the appropriate matrix elements of the transitions.

To incorporate these matrix elements in an approximate way we use the atomic cross sections of Yeh and Lindau [20] as multiplicative factors for the different partial DOS. For those partial DOS for which the equivalent atomic orbital is not occupied in the ground state, hence for which no cross sections can be found in the table of Yeh and Lindau, we use the corresponding cross section of the nearest atom in which this orbital *is* occupied. In table 7 we list the cross sections used in the calculation of the weighted DOS, which is shown in figure 9(*b*). Including these effects in the calculation brings it into better agreement with the experimental data: the relative contributions of the Te p- and s-like states have decreased; for the latter about right, for the former rather too much.

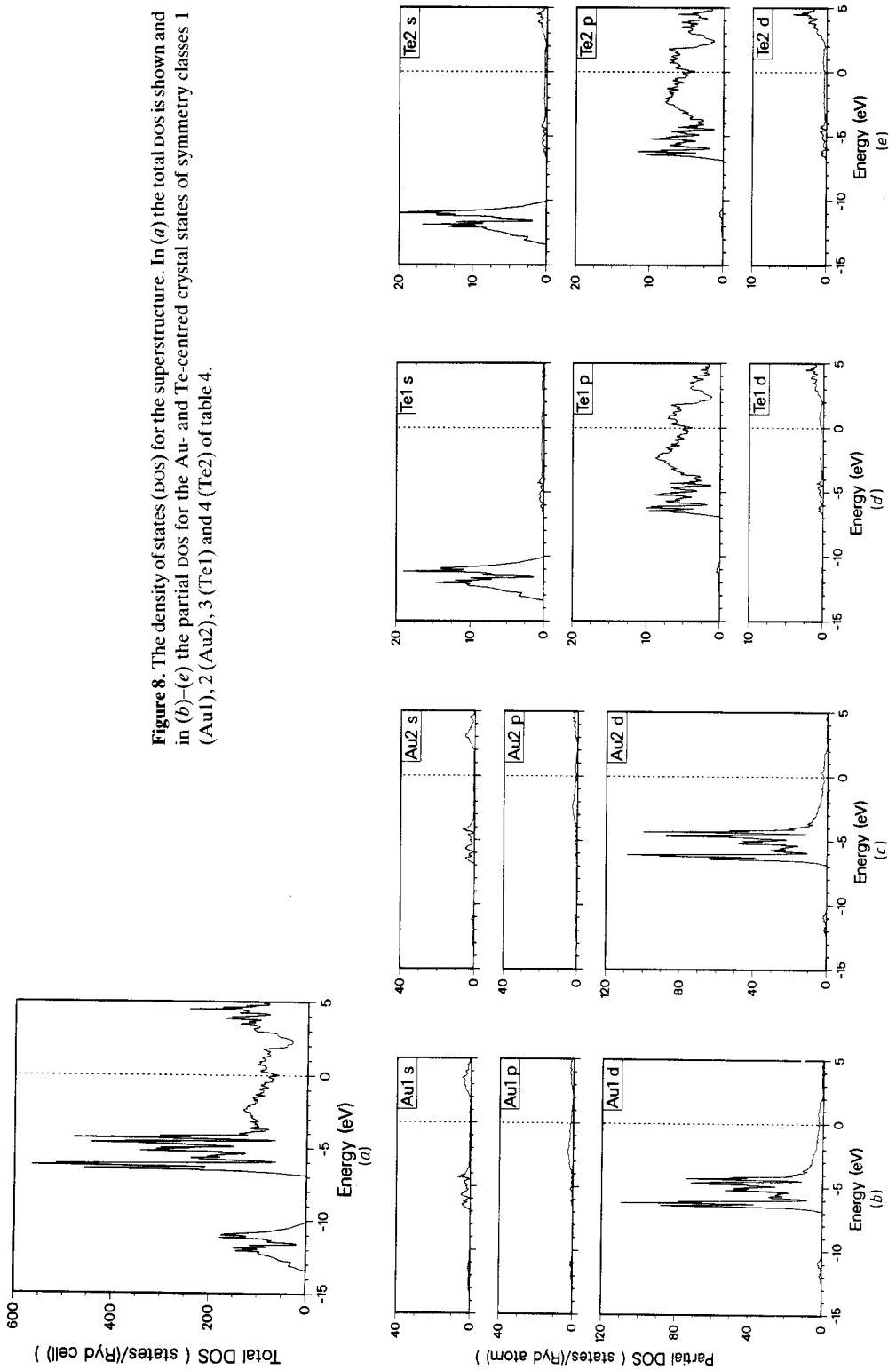

Figure 8. The density of states (DOS) for the superstructure. In (*a*) the total DOS is shown and in (*b*)–(*e*) the partial DOS for the Au- and Te-centred crystal states of symmetry classes 1 (Au1), 2 (Au2), 3 (Te1) and 4 (Te2) of table 4.

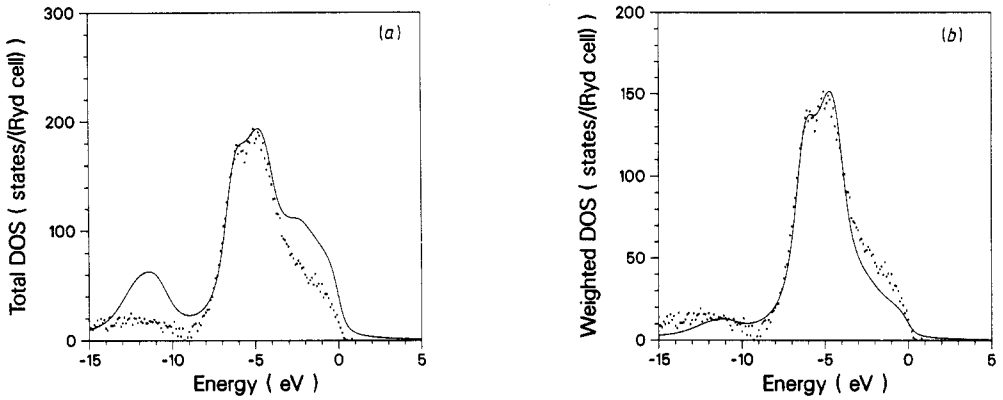

Figure 9. Experimental XPS valence spectrum (dots) and broadened total DOS of the superstructure (full curve) are shown in (*a*). For details of experiment and broadening, see text. The same experimental data are shown with the weighted total DOS in (*b*). The weights for the calculated DOS are taken from table 7.

Table 7. Scattering cross sections in kilobarns for the crystal functions derived from the closest corresponding atomic subshells and their cross sections for Al Kα radiation taken from [20].

Crystal function	Atomic shell	σ (kb)	σ/electron
Au 6s	Au $6s^1$	0.29	0.29
Au 6p	Tl $6p^1$	0.21	0.21
Au 5d	Au $5d^{10}$	26	2.6
Au 5f	Pa $5f^2$	8.0	4.0
Te 5s	Te $5s^2$	1.7	0.85
Te 5p	Te $5p^4$	2.6	0.65
Te 5d	La $5d^1$	0.76	0.76
Te 4f	Ce $4f^1$	2.2	2.2
e.s. 1s	H $1s^1$	0.0020	0.0020
e.s. 2p	B $2p^1$	0.0024	0.0024
e.s. 3d	Sc $3d^1$	0.053	0.053

We may conclude that the experimental valence XPS spectrum is explained quite well in terms of the calculated density-of-states and cross-section effects, and that a better quantitative agreement can probably be obtained by the explicit calculation of the transition matrix elements. Without the proper inclusion of these matrix elements it is certainly not possible to study the differences between calculated and experimental DOS that are due to the remaining structure approximation in the supercell.

7. The driving forces of the modulation

The understanding of the incommensurate modulation in calaverite is one of the goals of this paper. In the following subsections we will therefore study several possible

mechanisms for the modulation. First, we will explore the possibility that the modulation is a consequence of Fermi-surface nesting. Secondly, we will discuss the possibility that the modulation is connected with the existence of (static) mixed valencies for the gold atoms, as was suggested in previous publications [3, 5, 21]. Finally, we will study the driving forces of the modulation by comparing the energies involved in the average structure and in the superstructure. This comparison, a frozen phonon calculation, is made on the basis of Andersen's local force theorem, which relates the total energy difference of two self-consistent electron systems to a difference in Madelung energy and a difference in the sum of one-electron energies.

7.1. Fermi-surface nesting

One of the possible reasons for the instability of the average structure with respect to an incommensurate lattice deformation is the occurrence of Fermi-surface nesting. A model description and a criterion for the occurrence of a periodic lattice deformation and its accompanying charge-density wave have been provided by Chan and Heine [22], who formulate their model using the Fröhlich electron–lattice Hamiltonian in terms of a first-order electron–phonon coupling and a generalised electronic susceptibility. The criterion for the appearance of a periodic lattice deformation shows that the instability is favoured by a peak in the susceptibility at the wavevector of the modulation, as well as by a large electron–phonon coupling. If the Fermi surface contains flat pieces that can be brought together by a particular wavevector, the susceptibility shows a peak at this 'nesting' wavevector [23]. The flat pieces of Fermi surface lead to a peak in the DOS at the Fermi level. An example of a material showing an incommensurate lattice distortion due to Fermi-surface nesting is thought to be 1T-TaS_2 [24].

From the above considerations it is interesting to study the Fermi surface of the average structure and look for possible nesting. So energy contours were calculated on a set of planes parallel to the a^*c^* plane. A representative set of these contours for the bands 23/24 is shown in figure 10. Although all these planes clearly show structure in the $(-\boldsymbol{a}^* + \boldsymbol{c}^*)$ direction, which is approximately parallel to the wavevector of the modulation, there is no nesting to invoke an instability, and this is in agreement with the absence of clear peak structures in the DOS at the Fermi level. Also bands 25/26, which form small electron pockets at several places in the Brillouin zone, do not show any nesting.

We conclude that the instability of the average structure is not due to nesting of the Fermi surface. However, this does not imply the absence of a peak in the *susceptibility*, because this depends not only on the number of states available for transitions (large in the case of nesting) but also on the matrix elements of these transitions. Thus the instability can be due to the enhancement of the susceptibility by matrix element effects or by a large electron–phonon coupling.

7.2. Mixed valencies

The suggestion that the modulation in calaverite is connected with the appearance of mixed valencies of +1 and +3 for the Au atoms, as made in previous publications [3, 5, 21], was based on two analogies with other materials. First there are materials in which linear and square planar coordinations for Au exist. Examples are AuCl with a linear coordination and a valency for Au of +1 and $AuCl_3$ with square planar coordination and valency +3. Furthermore it is known that in transition-metal pyrites like

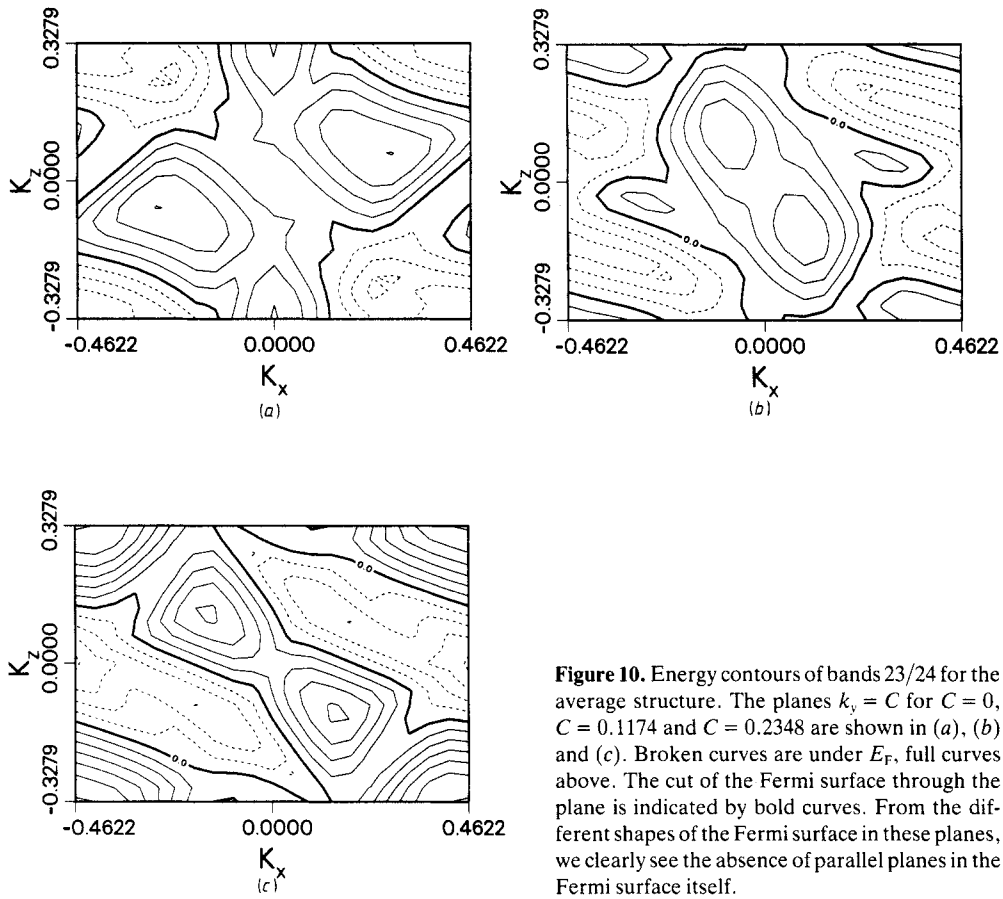

Figure 10. Energy contours of bands 23/24 for the average structure. The planes $k_y = C$ for $C = 0$, $C = 0.1174$ and $C = 0.2348$ are shown in (*a*), (*b*) and (*c*). Broken curves are under E_F, full curves above. The cut of the Fermi surface through the plane is indicated by bold curves. From the different shapes of the Fermi surface in these planes, we clearly see the absence of parallel planes in the Fermi surface itself.

FeS_2 the sulphur chains dimerise into S_2^{2-}. If (on average) such a dimerisation occurs in the Te chains of calaverite, the Au atoms would be forced into the unstable valency +2. This unstable valency could drive the system into a structure with modulated coordinations and valencies, which the extremes of the modulation correspond to the situations for Au in AuCl and in $AuCl_3$. Several observations seem to support this idea. Schutte and de Boer [5] mentioned that the reliability factor of their diffraction refinement procedure could be improved if they allow for silver substitution. The silver then prefers to sit in the linear coordinated positions, which is in agreement with the chemical stability of Ag^+ and the instability of Ag^{3+}. Finally we note that in sylvanite, $AuAgTe_4$, which is not modulated, the Ag atoms can be found in positions with a nearly linear coordination and the Au atoms in those with a square planar coordination.

The superstructure approximation for calaverite, described in secticon 3, is chosen in such a way that the extremal coordinations of the Au atoms in the incommensurate system are present. This and the local character of the effects of modulated coordinations suggest that mixed valencies, if present in the real system, will fall out of the superstructure calculation. The approximation to the crystal potential used in RASW is also unlikely to restrict the freedom of the valencies to modulate. The spherical averaging within the atomic spheres, of course, eliminates part of the difference between both Au

coordinations. However, the difference in the monopole contribution to the Madelung potential, which *is* taken properly into account, should lead to reliable predictions of the atomic monopole charge distribution in the crystal.

From the partial Au DOS of the average structure (figure 5(*b*)) it can be seen that the d-like states have only a very small tail extending through the Fermi level. It is therefore not surprising that the charge difference between both types of Au atomic spheres in the self-consistent superstructure is rather small (0.08 electrons, see table 6). This may not be very conclusive because of the arbitrary choice of the sphere radii in the crystal, but even if these radii are changed we do not find larger monopole differences. The partial occupation numbers per *l*-value also show no larger differences than the total charges. The non-spherical charge density will almost certainly show larger differences between the Au sites, but this is not immediately available from our calculation.

The absence of a significant difference in the valencies between the Au sites is also demonstrated by core-level studies. When we construct the potential of the superstructure from the rigidly shifted self-consistent charge densities of the average structure, the Madelung term in the potential introduces a difference at the sphere boundary of 0.2 eV between both types of Au sites due to their different coordinations. The core levels calculated with this (rigid) potential show, of course, a difference just equal to 0.2 eV. If we drive the system to self-consistency from this point, we observe that the potential difference at the sphere boundaries does not change significantly, because there is almost no charge flow between the different atomic spheres. However, within the atomic spheres the charge redistributes in order to screen the potential difference, and the final, self-consistent Au core levels differ by no more than 0.03 eV. For tellurium the differences between the core levels at symmetry-inequivalent sites are smaller than 0.05 eV.

The absence of significant core-level splitting predicted by our calculations is in agreement with the XPS data of van Triest *et al* [19], who observe no splitting for the Au core levels. For the Te levels they see an interesting phenomenon, which seems to fit in with the experience of other experimentalists [6]. There is a splitting of the Te states of several electronvolts, which is angle- and time-dependent and therefore attributed to a surface reconstruction following the scraping of the sample surface. The size of the splitting as well as the angle and time dependence exclude the possibility that the splitting is a bulk (ground-state) effect.

We can conclude from the preceding that the differences in coordination of both types of Au positions do not lead to observable core-level splitting, nor to substantial charge transfer, in contradiction with the predictions of the mixed valence model. It might, however, be possible to connect the remarkable observations concerning the coordinations and the preferences of gold and silver for different coordinations with an energy gain due to a modulated covalency in the bonding. In order to study that idea, it would be interesting to calculate the non-spherical charge-density distribution for both the average structure and the superstructure.

7.3. Energetics of the modulation

The obvious way to study the origin of the modulation is to compare the total energies of the average structure and the superstructure. However, it is well known that calculational methods like the one we use in this paper, based on the rather crude atomic sphere approximation to the crystal potential, do not give reliable phonon frequencies. One way to avoid the typical problems of such a comparison and to obtain qualitatively

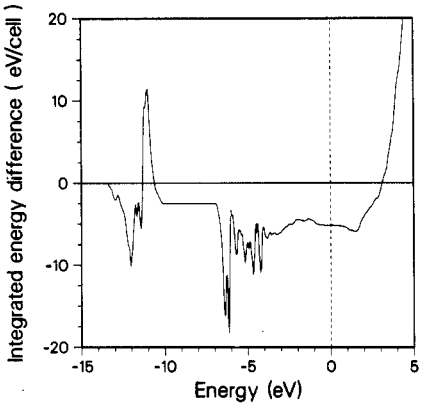

Figure 11. Integrated one-electron energy difference between superstructure and average structure (see text). The energy difference is calculated per superstructure unit cell. The Fermi level is indicated by the vertical broken line.

correct results is to use Andersen's local force theorem [25]. This theorem relates the difference in the total energies of two self-consistent structures to the difference in the sum of the one-electron energies between the undisturbed self-consistent system and a system with this self-consistent potential rigidly shifted according to the perturbation, plus a simple electrostatic term for the change in the Madelung energy. The theorem is correct to second order in the charge-density difference. Since the charge-density difference between the average structure and the superstructure is very small, we expect that a calculation making use of the local force theorem will give qualitatively correct results.

First we calculate with the rigidly shifted potential the Madelung contribution to the energy difference. This turns out to be approximately 0.3 eV per superstructure unit cell, stabilising the average structure. The small value of the difference is due to the relative neutrality of the atomic spheres as well as the large interatomic distances of the atoms that participate in the modulation. As observed before, the sphere radii are rather arbitrary, but if they are changed the electrostatic term remains very small. The one-electron term of the energy difference was calculated from the difference in DOS. The result can be seen most clearly from a plot of the integrated energy difference $\Delta(E)$, given by

$$\Delta(E) = \int_{-\infty}^{E} \mathrm{d}\varepsilon\, \varepsilon[g_{SS}(\varepsilon) - g_{AS}(\varepsilon)]$$

where g_{SS} and g_{AS} denote the DOS of the superstructure and the average structure respectively, and both DOS are taken per superstructure unit cell. The plot of $\Delta(E)$ is shown in figure 11. First of all it can be noted that the energy difference has the correct sign, favouring the superstructure, and is much larger than the opposing electrostatic term. The superstructure is in total more stable by 5.2 eV, i.e. about 0.5 eV per atom. Remarkably enough the energy gain comes mostly from states quite far from E_F, and is almost equally distributed between the Te s-like states and the (Te p–Au d) complex. These observations are in agreement with the absence of Fermi-surface nesting and they are not in contradiction with the modulated covalency suggested in the previous section.

8. Conclusions

We have used conventional band-structure techniques to study the electrons in two approximate crystal structures of incommensurately modulated calaverite, namely the

average structure and a commensurate superstructure. The energy bands, the density of states and the occupation numbers for both structures have been compared. The density of states for the superstructure compares very well with experimental XPS data. Since the differences between both structures for the physical quantities mentioned above are small, it does not seem necessary to calculate higher-order periodic structure approximations. It has been observed, however, that the Fermi surface is very sensitive to the exact form of the modulation. With the techniques applied in this paper it is practically impossible to access higher-order approximations, because the next simplest structure approximation would have a wavevector $\boldsymbol{q} = -\frac{2}{5}\boldsymbol{a}^* + \frac{1}{2}\boldsymbol{c}^*$, with 60 atomic spheres in the unit cell, while the next order of the continued-fraction expansion would give $\boldsymbol{q} = -\frac{2}{5}\boldsymbol{a}^* + \frac{4}{9}\boldsymbol{c}^*$ with as many as 270 atomic spheres in the unit cell.

As far as the driving forces for the modulation are concerned, we have discussed several models. We conclude that the previously proposed connection with mixed valencies for the Au atoms is not valid, and we have shown the absence of Fermi-surface nesting. Furthermore, we have provided a qualitative indication for the instability of the average structure by the comparison of one-electron energy sums and an electrostatic energy difference making use of Andersen's local force theorem. While the small electrostatic term tends to stabilise the average structure, the one-electron energy difference is much larger and stabilises the superstructure with approximately 0.5 eV per atom. The integrated one-electron energy difference suggests that the origin of the modulation involves both the Te s-like states and the (Te p–Au d) complex. Finally we conclude that the remarkable observations concerning the coordinations of the gold and silver atoms in calaverite as well as sylvanite are not a consequence of energy gain by an actual valence modulation, but could possibly find their origin in an energy gain due to a modulated covalency. To verify this idea we hope to perform calculations of the non-spherical charge density for both structures.

Acknowledgments

The authors would like to thank C Haas, A G M Janner and H L M Meekes for stimulating discussions and A van Triest for the XPS data.

References

[1] van Tendeloo G, Gregroriades P and Amelinckx J 1983 *J. Solid State Chem.* **50** 321
[2] Dam B, Janner A and Donnay J 1985 *Phys. Rev. Lett.* **55** 2301
[3] Krutzen B 1988 *Fractals, Quasicrystals, Chaos, Knots and Algebraic Quantum Mechanics* ed A Amann (Dordrecht: Kluwer) p 139
[4] Janssen T and Janner A 1987 *Adv. Phys.* **36** 519
[5] Schutte W and de Boer J 1988 *Acta Crystallogr.* B **54** 486
[6] Dijkstra E, Kremers M and Devillers M 1989 *Z. Phys.* B **76** 487
[7] Janner A and Dam B 1989 *Acta Crystallogr.* A **45** 115
[8] Penfield F and Ford W 1902 *Z. Krist. Min.* **35** 430
[9] Smith H 1903 *Z. Krist. Min.* **37** 209
[10] Harvey R 1928 *Econ. Geol.* **23** 778
[11] Donnay J 1935 *Annales de la Société Géologique de Belgique* vol 18
[12] Takeda T 1979 *J. Phys. F: Met. Phys.* **9** 815
[13] Williams A, Kübler J and Gelatt C D Jr 1979 *Phys. Rev.* B **19** 6094
[14] Nemoshkalenko V V, Krasovskii A E, Antonov V N, Antonov Vl N, Fleck U, Wonn H and Ziesche P 1983 *Phys. Status Solidi* b **120** 283

[15] Krutzen B and Springelkamp F 1989 *J. Phys: Condens. Matter* **1** 8369
[16] Perdew J and Zunger A 1981 *Phys. Rev.* B **23** 5048
[17] Ceperley D and Alder B 1980 *Phys. Rev. Lett.* **45** 566
[18] Tunnel G and Pauling L 1952 *Acta Crystallogr.* **5** 375
[19] van Triest A private communication
[20] Yeh J and Lindau I 1985 *At. Data Nucl. Data Tables* **32** 1
[21] de Groot R, Gutfreund H and Weger M 1987 *Solid State Commun.* **63** 451
[22] Chan S-K and Heine V 1973 *J. Phys. F: Met. Phys.* **3** 795
[23] Evenson W, Flemming G and Liu S 1973 *Phys. Rev.* **178** 930
[24] Inglesfield J E 1980 *J. Phys. C: Solid State Phys.* **13** 17
[25] Heine V 1980 *Solid State Physics* vol 35, ed H Ehrenreich, F Seitz and D Turnbull (New York: Academic) p 1